Hindawi
Advances in Materials Science and Engineering
Volume 2022, Article ID 2240624, 15 pages
https://doi.org/10.1155/2022/2240624

Research Article

Experimental Research on Waste Fiber Recycled Concrete Beam-to-Column Joints under Monotonic Loading

Jinghai Zhou,[1] Liwei Jin,[1] Jingtong Qu,[1] Hong Sun,[1] Tianbei Kang,[2] Ye Yuan,[1] and Yu Liu[1]

[1]*School of Civil Engineering, Shenyang Jianzhu University, Shenyang, China*
[2]*Key Laboratory of Intelligent Management for Transport Infrastructure in Xi'an, Xi'an, China*

Correspondence should be addressed to Tianbei Kang; kangtianbei@sjzu.edu.cn

Received 15 November 2021; Revised 14 January 2022; Accepted 1 February 2022; Published 12 March 2022

Academic Editor: Luigi Di Sarno

The mechanical properties, failure forms, and deformation characteristics of 10 beam-to-column joints under monotonic loads were compared and analyzed. The design variables were waste fiber content (0.08%, 0.12%, and 0.16%), waste fiber length (12 mm, 19 mm, and 30 mm), and replacement rate of recycled aggregates (0%, 50%, and 100%). The results indicated that, under an axial compression ratio of 0.4, all specimens underwent plastic hinge failure at the beam end under monotonic loading and experienced four stages of the initial cracking, full-cracking, limit, and failure stages. There was no shear oblique crack in the core area of the joint, and no shear failure occurred. When the replacement of recycled aggregates is 50%, the tensile strength of concrete mixed with a specific amount of fibers can be effectively improved. The ultimate bearing capacity of the beam end is improved when the length and volume of the waste fibers are 19 mm and 0.12%, respectively. The ratios between the calculated and tested ultimate bearing capacity of beam-column joints are in the 0.99–1.10 range, and the calculated and tested values are in good agreement.

1. Introduction

The construction industry in China is facing two serious problems: the huge consumption of natural resources (such as sand and gravel) [1] and the quantity of construction and demolition waste [2]. Waste concrete accounts for 30–50% of construction and demolition waste. The recycling of waste concrete can effectively address these two serious problems. The environmental benefits in using the recycled coarse aggregates (RCA) as a substitute for natural coarse aggregates (NCA) for the production new concrete open, the new path for the construction industry. Xiao et al. [3] used a road engineering example in Shanghai and demonstrated that it is feasible to apply recycled concrete with a replacement rate of 50% to the pavement. Meng et al. [4] proposed a mixing ratio design method for recycled aggregate concrete based on strength, with a design strength ranging from 30 to 50 MPa, and a RCA replacement rate ranging from 20 to 100%. Etxeberria et al. [5] and Poon et al. [6] reported the relationship between the replacement rate of RCA and the strength of concrete. When the replacement rate of RCA is less than 50%, the strength of the recycled concrete is close to that of ordinary concrete. However, the strength value decreased significantly because the replacement rate of the RCA was greater than 50%. The shortcomings of recycled concrete can be limited by adding various fibers, such as steel [7], polymeric [8], and waste fibers [9], etc. The addition of fibers can inhibit the development of cracks in the cement matrix and improve the strength of the recycled concrete. These results provide a basis for the application of recycled concrete to structural components.

Beam-to-column joints are the most seismic-prone elements in a framed structure that is generally designed for gravity loads [10, 11]. The beam-to-column joints are divided into corner, edge, and intermediate joints according to their position in the frame. Numerous studies have been conducted on the bearing behaviors of concrete beam-to-column joints under monotonic and cyclic loading. Nehdi et al. [12] proposed a shape memory alloy fiber-reinforced polymer (FRP) hybrid RCA concrete beam-column joint by using a FRP as a reinforcing material and subsequently conducted experiments on the middle joint of the beam-

column under reversed cyclic loading. Najafgholipour and Arabi [13] used finite element modeling technology to establish the ultimate shear strength formula corresponding to the core tensile strength of the computing node and implemented the model in SAP2000 (a nonlinear framework analysis software). Marthong et al. [14] studied the effect of micro-concrete addition on the performance of RCA concrete beam-to-column joints under cyclic loading. The results showed that the use of micro-concrete can significantly improve the seismic performance of recycled concrete beam-to-column joints. In addition, the seismic performance of middle joints in frame beams and columns under different conditions has been studied [15–19]. Experiments demonstrated that the joints in the frame exhibited good seismic performance after reinforcement or repair.

The results of these studies demonstrated that the performance of fiber-reinforced concrete is significantly affected by parameters such as fiber type, fiber fractions, concrete strength, and loading condition. Su et al. [20] measured the shear bearing capacity of the core area of four high-toughness fiber-reinforced concrete frame joints under cyclic loading and found that adding high-toughness fiber can effectively control the number of cracks at the core area of the joint, and Du and Wang [21] also reached the same conclusion. Candido and Micelli [22] used fiber-reinforced concrete materials to reinforce conventional reinforced concrete frame structures in key areas and performed a large number of nonlinear static and dynamic analyses with distributed plasticity. Wang et al. [23], Hany et al. [24], Ghomi and El-Salakawy [25], and Saqan et al. [26] also used fiber-reinforced polymer composite materials repair and strengthen concrete beam-column joints. Further, it was found that the shear resistance and seismic performance of concrete beam-column joints reinforced by FRP, CFRP, and other materials are improved. However, research on waste fiber-reinforced recycled concrete beam-to-column joints subjected to monotonic loading from earthquakes has not been undertaken so far.

In this study, the mechanical properties, failure forms, and deformation characteristics of 10 beam-to-column joints under monotonic loads were compared and analyzed. The design variables were waste fiber content (0.08%, 0.12%, and 0.16%), waste fiber length (12 mm, 19 mm, and 30 mm), and replacement rate of RCA (0%, 50%, and 100%). In addition, a calculation method for the ultimate bearing capacity of a beam-to-column joint was proposed.

2. Experimental Program

2.1. Materials. The cement used in this study was ordinary Portland cement (P.O 42.5). Fine aggregates were natural river sand with a fineness modulus of 2.8, the water content was 4.14%, and apparent density was 2620 kg/m^3, following Chinese standard GB 50164. The grading of fine aggregates is listed in Table 1. There were two kinds of coarse aggregates, one of which was the NCA and the other was the RCA, and the particle sizes of the two aggregates were 5–25 mm. The RCA from the abandoned concrete beams with the strength of C40 was produced after crushing and screening by the jaw crusher. The properties of the coarse aggregates are shown in Table 2, following Chinese standard GB/T 14685. The grain size distribution curves of the coarse aggregates are shown in Figure 1.

Table 1: The sample sieve analysis of sand.

Aperture size/mm	4.75	2.36	1.18	0.6	0.3	0.15	0.075	End
Screening residue/%	3.6	5.4	8.9	25	43.46	10.4	2.04	1
Accumulated residue/%	3.6	9.0	17.9	42.9	86.36	96.86	99	100

Waste fibers came from the abandoned carpets and the chemical composition was polypropylene. The waste carpet was manually split into waste fibers with the length of 12 mm, 19 mm, and 30 mm, respectively. The water absorption of the waste fibers is less than 1%. The density of the waste fibers is 0.91 g/cm^3, which is tested by the liquid displacement technique, according to JC/T 287-2010 (Chinese standard). The elastic modulus of the waste fibers is 3.79×10^3 MPa and the ultimate elongation is 1.73%. The preparation of waste fibers is described in Figure 2.

2.2. Mixture Proportions. The percentage of mixing mass of the coarse aggregates, sand, and water was determined by the laboratory test. The design variables of the experiment were replacement rate of RCA (0%, 50%, and 100%), waste fiber volume fraction (0%, 0.08%, 0.12%, and 0.16%), and the length of waste fibers (12 mm, 19 mm, and 30 mm). The mixing water consisted of free water and additional water in accordance with JGJ/T 443-2018 (Chinese standard). The free water was a hydration reaction with cement, while the additional water was to reduce the influence of the large water absorption of RCA (see Table 2). Cube and axial compressive strengths were performed with the HYE-2000 Electric-Liquid Pressure Experimental and in accordance with GB/T 50081 (Chinese standard), three parallel specimens were made for each specimen ID. The material mixtures of the samples are shown in Table 3.

To prepare the waste fiber recycled concrete, coarse aggregates, and waste fibers were mixed for 2 min in a forced concrete mixer, and then the cement and water were added and stirred at low speed for 2-3 min to achieve good workability, according to the GB/T 50081 (Chinese standard).

2.3. Specimen Preparation. A series of 10 beam-to-column joints with the same dimensions and reinforcement were prepared for the test, according to GB 50010-2010 (Chinese standard). The dimensions and details of the specimens are shown in Figure 3, and the material properties of the reinforcement are listed in Table 4. Two intersecting displacement meters were arranged at the joint to measure shear deformation in the core region. Eight reinforcement strain gauges were arranged diagonally to measure the shear deformation of the stirrup in the core region of the joint. Two identical concrete strain gauges were arranged on the

Table 2: Basic material properties of coarse aggregates.

Type	Apparent density/kg·m^{-3}	Bulk density/kg·m^{-3}	Water absorption/%	Crush index/%
NCA	2730	1853	1.2	6.4
RCA	2461	1167.6	4.18	17

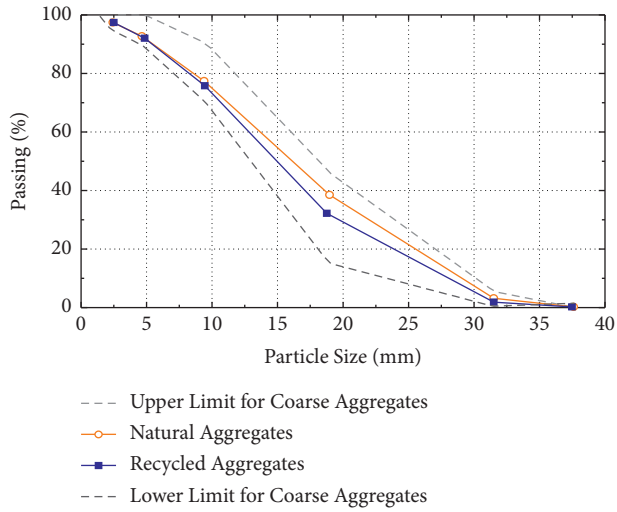

Figure 1: Coarse aggregates gradating curves.

Figure 2: The preparation of waste fibers.

upper part of the beam, approximately 20 mm from the root of the beam. Three equally spaced concrete strain gauges were vertically attached to the cross-sectional surface of the front beam, approximately 20 mm from the root of the beam. Six concrete strain gauges in the 45° direction were arranged at the core area of the joint. The displacement meters, reinforcement layout, and concrete strain gauges in the joint area are shown in Figure 4.

2.4. Equipment and Loading System. The field loading and schematic of loading device are shown in Figures 5 and 6. A 5000 kN oil hydraulic jack (see Figure 6(a)) was arranged at the top of the column to apply axial force, and the axial compression ratio was 0.4. An oil hydraulic jack with a range of 600 kN was installed at the beam, as shown in Figure 6(b), to apply a vertical anti-symmetric load. To prevent tilting instability of the specimen during loading, the lateral support was set at the top of the column end (see Figure 6(c)). Meanwhile, a force sensor with a range of 100 kN was installed (see Figure 6(d)), to measure the lateral force generated during static loading. The entire process of the experiment was controlled by a computer, and electronic readings were used for all types of test instruments.

A force-control loading system was employed in this experiment. The loading method involved applying a constant axial force at the top of the column while applying an anti-symmetric vertical load to the beam end. A constant axial force was applied to the top of the column, the axial pressure ratio was approximately constant by adjusting the oil pump during the test, and the axial pressure ratio was 0.4. The test was divided into two stages: including preloading

Table 3: Mixture proportion and compression strength.

Specimen ID	Cement/ kg·m^{-3}	Sand/ kg·m^{-3}	NCA/ kg·m^{-3}	RCA/ kg·m^{-3}	Water/ kg·m^{-3}	Cube compressive strength $f_{cu,k}$/N·mm^{-2}	Axial compressive strength f_{ck}/N·mm^{-2}
NCJ	390	709	1156	0	195	43.77	29.24
RCJ-19-0.12	390	709	1156	0	195	43.75	29.23
RCJ-50-12-0.12	390	709	578	578	205	43.71	29.22
RCJ-50-19-0.12	390	709	578	578	205	43.70	29.22
RCJ-50-30-0.12	390	709	578	578	205	43.70	29.22
RCJ-50-19-0.08	390	709	578	578	205	43.69	29.22
RCJ-50-19-0.16	390	709	578	578	205	43.70	29.22
RCJ-100-19-0.12	390	709	0	1156	215	43.64	29.19
RCJ-100-19-0.12	390	709	0	1156	215	43.64	29.19
RCJ-100-19-0.12	390	709	0	1156	215	43.64	29.19

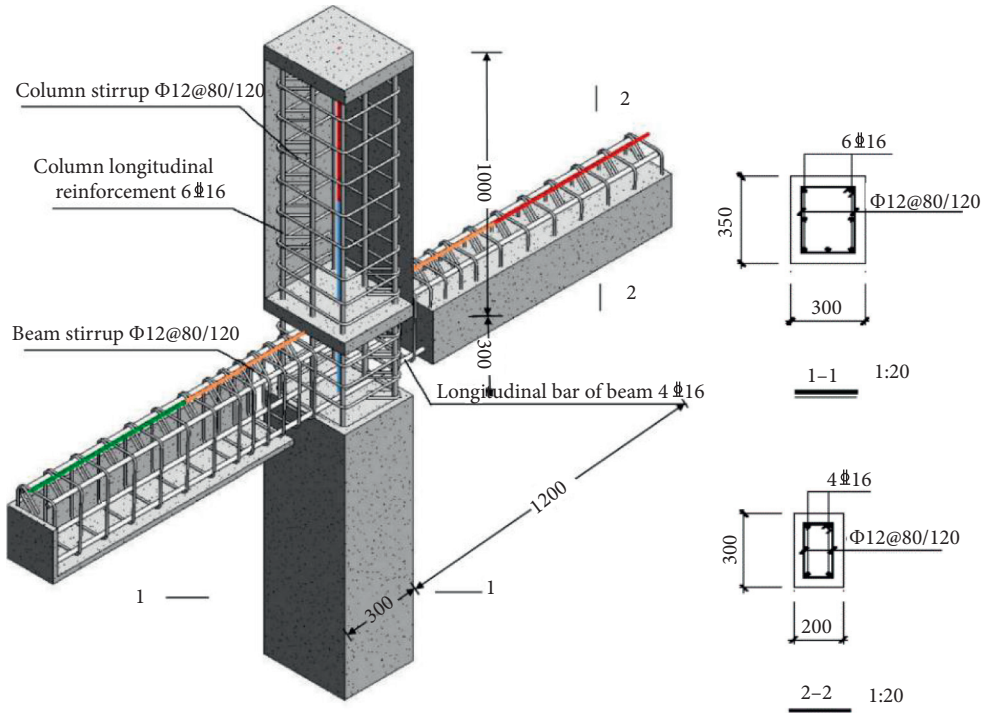

Figure 3: Dimensions and reinforcement details of specimens.

Table 4: Mechanical properties of steel bar.

Reinforcement specification	Yield strength fy (N/mm^2)	Ultimate strength fu (N/mm^2)	Stirrup fu (×105 N/mm^2)
Φ8 stirrup	311.8	454.4	2.27
16 longitudinal	335	455	2

and formal loading. There were three preloading stages with 0.6 tons per stage. During the formal loading, the load of each grade was approximately 1/15 of the ultimate load in the early stage, 1/30 of the ultimate load in the middle stage, and 1/60 of the ultimate load in the late stage until the specimen was destroyed. When the load-displacement curves of the beam end exhibited a clear inflection point, the specimen was considered to be yielding.

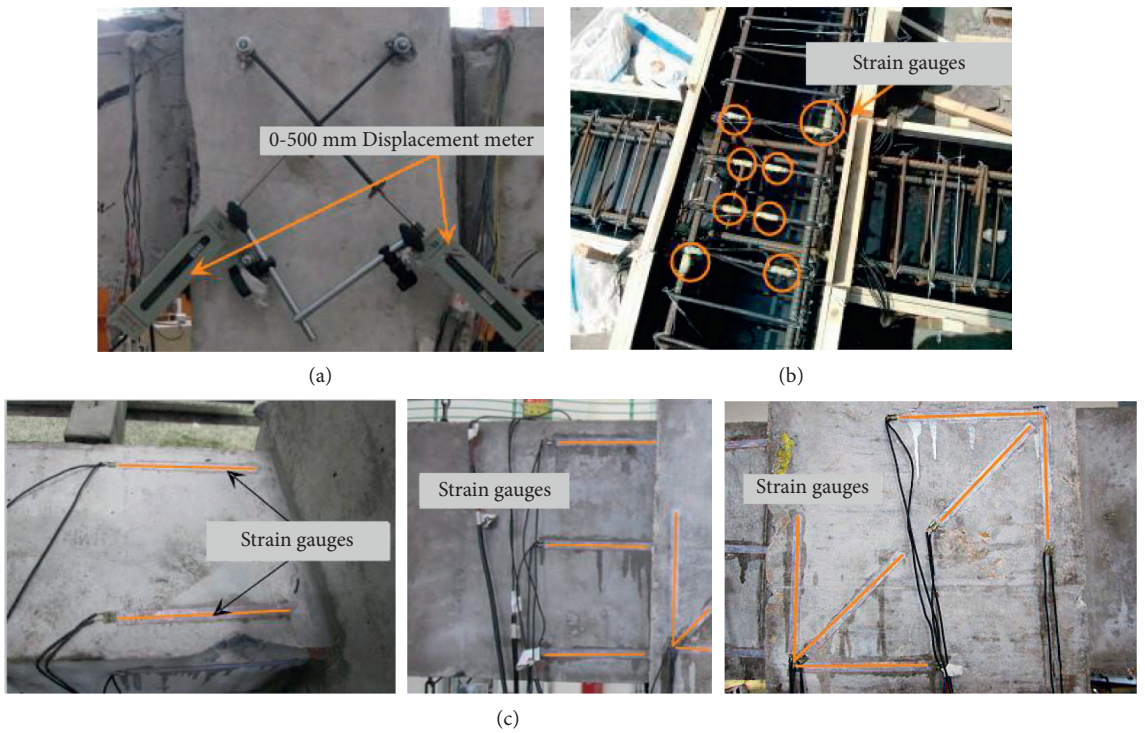

Figure 4: Arrangement of displacement meters and strain gauges. (a) Displacement meters. (b) Strain gauges of stirrup. (c) Concrete strain gauges.

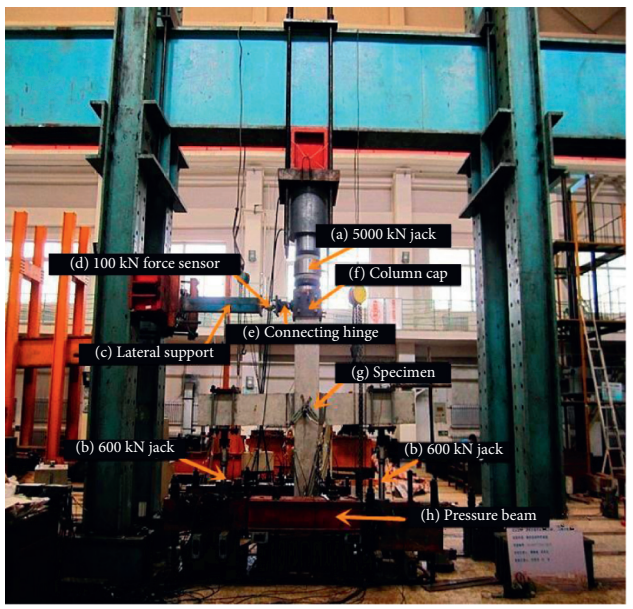

Figure 5: Field loading.

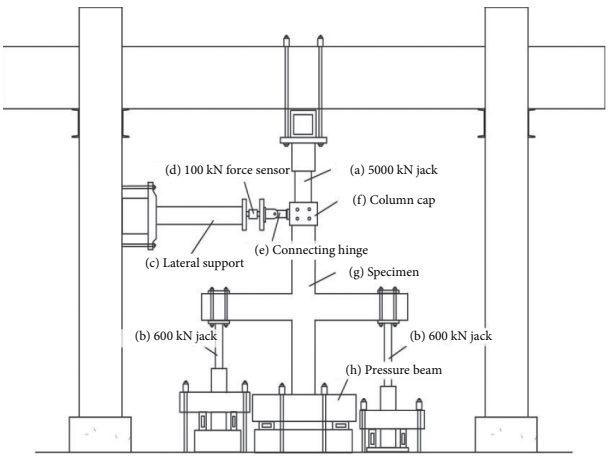

Figure 6: The schematic of loading device.

3. Experimental Phenomena

The failure mode was the bending failure of the beam end, and it was similar for all the joints. Three representative beam-to-column joints (NCJ, RCJ-50-19-0.12, and RCJ-100-19-0.12) were selected for analysis, and their failure morphology is shown in Figure 7. At the beginning of the stress loading, there were several micro-fractures in the beam along its length. As the load gradually increased, the initial width of the crack increased slowly, but the height gradually increased. There are continuous new cracks at the beam end in the joint core area. With an increase in the load, cracks appeared near the root of the beam; thereafter, all the cracks in the beam penetrated up and down. Meanwhile, the specimens reached the yield stage, as shown in Figure 7(a). Second, as the load increased, the concrete in the joint core area remained intact without shearing diagonal cracks and there were no new vertical cracks on the beam. The vertical cracks at the beam-column interface and the original cracks on the beam continued to develop, as shown in Figure 7(b). Third, with continuous loading, the concrete at the beam-

Figure 7: Experimental phenomena. (a) Yielding stage. (b) Ultimate stage. (c) Maximum crack width of beam end. (d) Joint form under failure load.

column interface was crushed, and the vertical cracks at the beam end increased rapidly. The bearing capacity of the specimen reached its limit, and the concrete at the beam end was fully cracked. The concrete exited the work, and the longitudinal reinforcement of the beam continued to bear the deformation. The maximum strain value of the horizontal stirrup in the joint core was lower than the yield strain of the stirrup, indicating that the horizontal stirrup in the joint core area did not yield and could still bear the shear force in the joint area (see Figure 7(c)). Finally, during the unloading process, the bearing capacity of the specimen decreased rapidly. The concrete in the compressive region at the beam end was severely crushed, and the concrete cover continued to spall. The width of the crack was approximately 7–10 mm, as shown in Figure 7(d). The specimen creates huge noise, and it can be

considered that the test piece has been damaged; however, the loading process is completed.

4. Results and Discussion

4.1. Load-Displacement Curve of the Beam End. The load-displacement curves of the beam-to-column joints are shown in Figure 8. The curves of the specimens are similar and can be divided into three stages: elastic, yield, and failure stages. The axial compression ratios of specimens RCJ-19-0.12, RCJ-50-19-0.12, and RCJ-100-19-0.12 were 0.4, the amount of waste fibers was 0.12%, the length of the waste fibers was 19 mm, and the replacement rates of the RCA were 0%, 50%, and 100%, respectively.

Figure 8 shows that, in the elastic stage, the load-displacement curves of the push and pull sides coincide, and the RCA have no significant effect on the elastic stage. With the increase in load, the specimen with RCA enters the yield stage faster than the NCJ. The ultimate bearing capacity of RCJ-50-19-0.12 was 9.6% and 11.22% higher than those of RCJ-19-0.12 and RCJ-100-19-0.12, respectively, which are close to that of NCJ. The main reason is that there is better compatibility between RCA and fresh cement slurry, and each of these has the possibility of chemical reaction. The surface of the RCA is rough and the interface meshing ability is strong, thereby improving the performance of the interface to a certain extent. In addition, the RCA have a high water absorption rate and can absorb excess water in the cement mortar, which not only reduces the surface water-cement ratio of the aggregates but also reduces the effective water-cement ratio of the concrete mixture, thereby increasing the strength of the recycled concrete. It is shown that, as the replacement rate of RCA increases in a specific range, the ductility and bearing capacity of recycled concrete beams also decrease.

Figure 9 represents that the load-displacement curves of waster fiber recycled concrete specimens. Fibers can effectively prevent the development of concrete cracks, thereby increasing the strength and toughness of the concrete [7–9]. As shown in Figure 9(a), when the amount of waste fibers was 0.12%, the yield load of the beam end in the joint area was greater than the yield load of 0.08% and 0.16% content of the waste fibers, and it increased by 14.1% and 2.82%, respectively. It can be deduced from Figure 9(b) that the length of the waste fibers is 19 mm and the yield load of the beam end in the joint area is 40 kN, which is 12.04% and 4.44% higher than the yield load of the waste fibers with the lengths of 12 mm and 19 mm, respectively. When the length of the waste fibers is 19 mm, the ultimate bearing capacity of the beam end in the joint area is 52.5 kN, which is 22.09% and 12.66% higher than the ultimate bearing capacity of the waste fiber length of 12 mm and 19 mm, respectively. The addition of waste fibers can alleviate the stress concentration generated, and the fibers across the cracks inhibit the continuous development of these cracks (see Figure 10).

4.2. Characteristic Load. Figure 11 shows the cracking load P_{cr}, yield load P_y, ultimate load P_u, and failure load P_m of the specimens; it also shows the characteristic load of the specimens with the replacement rate of the RCA. When the RCA content was 50%, the characteristic load of specimen RCJ-50-19-0.12 was higher than that of RCJ-100-19-0.12, and it was close to that of the standard specimen NCJ. This is mainly because the addition of RCA is unfavorable to the ultimate bearing capacity of the beam end. As the amount of RCA increased, the ultimate bearing capacity of the beam end decreased. As the "secondary reinforcement" of concrete, waste fiber is pulled out during the process of beam end failure, which consumes part of the energy of concrete in the joint core area and thereafter improves the ultimate bearing capacity of the beam end. There is a reasonable volume of waster fibers; when the volume of waste fibers is 0.08% and 0.16%, the volume of fibers is insufficient or excess, and both the ultimate bearing capacity and strength will be reduced, as shown in Figure 11(b). When the fiber length is 19 mm, the ultimate load-bearing performance of the beam end is the best, as shown in Figure 11(c). The ultimate load of specimen RCJ-50-19-0.12 is significantly higher than those of the specimens RCJ-50-12 -0.12 and RCJ-50-30-0.12, and is very close to that of NCJ.

4.3. Shear Deformation-Load Curve of the Core Area. Under the action of horizontal shear, the concrete in the core area will crack due to its oblique tension, and the core area of the joint will produce shear deformation; Karayannis and Golias [27, 28] reached the same conclusion. No shear failure occurred in the core area, and the failure of the specimen was bending failures at the end of the beam, which conformed to the design principle of "strong nodes and week members" in accordance with GB50010-2010 (Chinese standard). The shear angle is calculated by measuring the change of diagonal length in the beam-column core (see Figure 12).

The value of the shear angle can be calculated based on

$$\gamma = \frac{\sqrt{a^2 + b^2}}{ab} \cdot \frac{\left|\delta_1 + \delta_2\right| + \left|\delta_3 + \delta_4\right|}{2}. \quad (1)$$

where δ_1, δ_2, δ_3, and δ_4 represent the variations in the length. Shear deformation-load curves of specimens are shown in Figure 13.

Due to the fact that a plastic hinge is formed at the beam end, the load cannot be effectively transmitted to the joint area. Concrete in the joint area does not crack when the specimen is damaged. The node is still in the elastic stage, and concrete bears the shear resistance. As shown in Figure 13, the shear deformation-load curves of the specimens are roughly linear compared with the specimens with different replacement rate RCA, waste fiber length, and volume incorporation. When the shear angle is less than 3×10^{-3} rad, the curves of specimens tend to steep. The growth rate of the curves in Figure 13(a) and Figure 13(c) slows down with the load reaches about 30 kN. The trend of the curves in Figure 13(b) is relatively flat after the load reaches about 40 kN. The volume of waste fibers has a great influence on the shear deformation-load curve of the joint core area.

Fibers can improve beam shear failure deformation and enhance concrete ductility, which is mainly reflected in three aspects. On the one hand, fibers can replace or partially

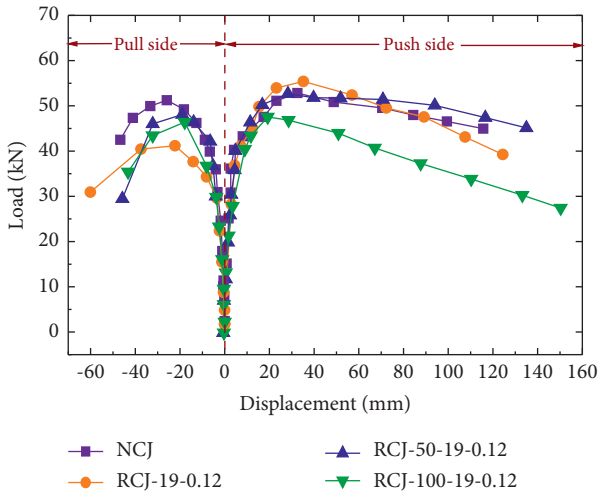

Figure 8: Load-displacement curves of specimens with different replacement rate of RCA.

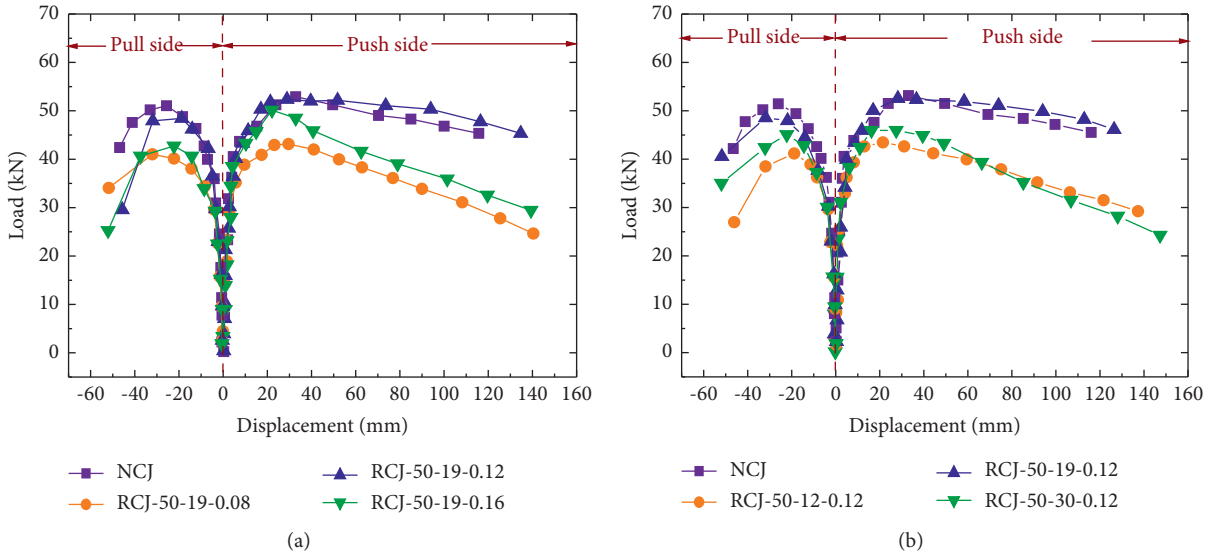

Figure 9: Load-displacement curves of waste fiber concrete specimens. (a) Volume of waste fibers. (b) Length of waste fibers.

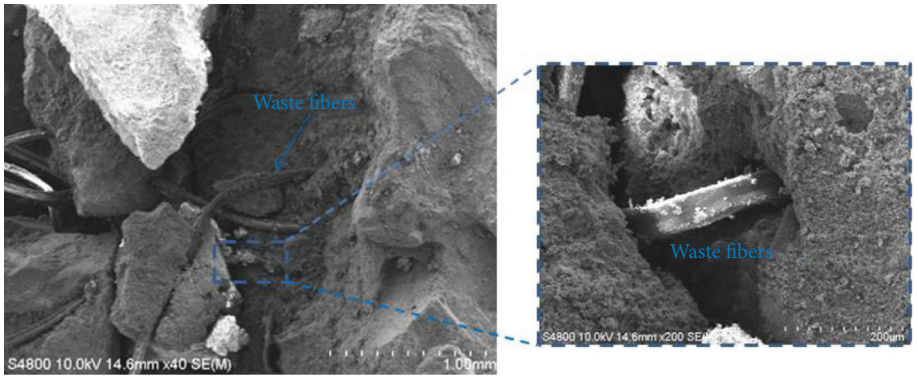

Figure 10: Micromorphology of waste fibers.

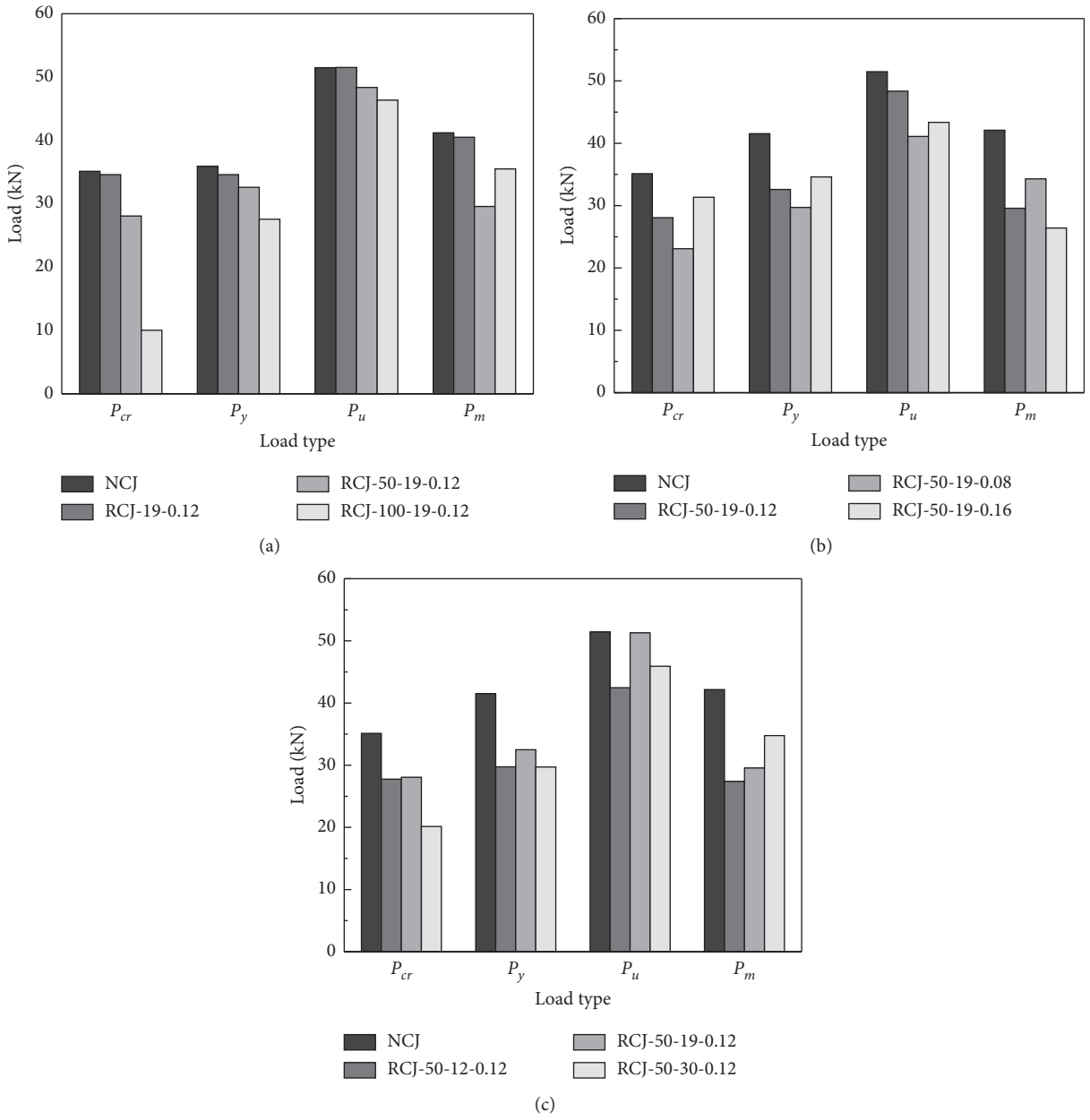

Figure 11: Comparison of influencing factors of characteristic load. (a) Replacement rate of RCA. (b) Volume of waste fibers. (c) Length of waste fibers.

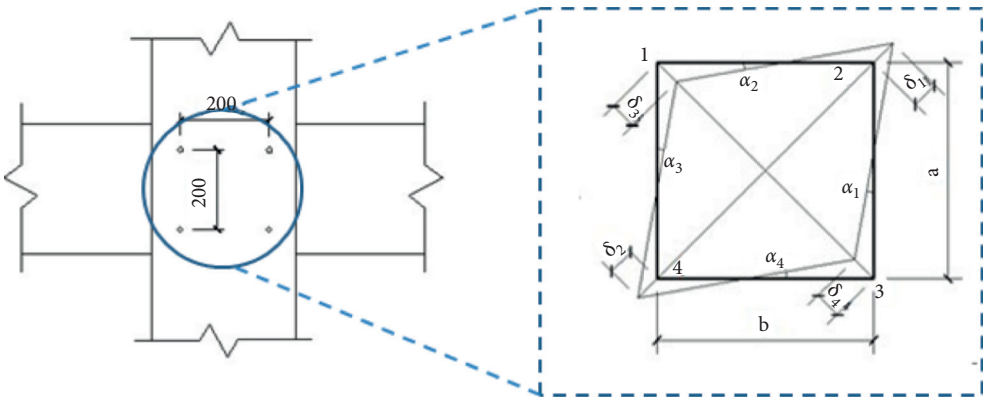

Figure 12: Measure of joint cores shearing deformation.

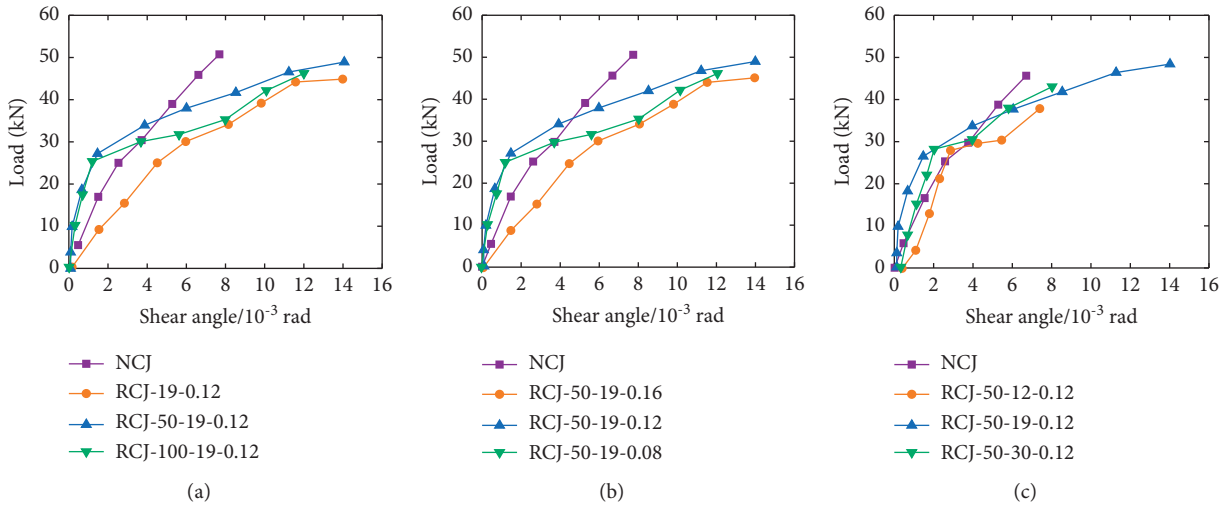

Figure 13: Shear deformation-load curve. (a) Replacement rate of RCA. (b) Volume of waste fibers. (c) Length of waste fibers.

replace the shear resistance of stirrups. On the other hand, fibers improve the toughness of concrete and significantly increase the shear compression zone of the ultimate compressive strain and deformation capacity of concrete. When the oblique section cracks, the fibers bear the stress released by the concrete and restrict the development of oblique cracks, which enhances the occlusion of the aggregates and relieves the suddenness of destruction to a certain extent. Finally, fibers strengthen the bond between concrete and steel.

4.4. Rebar Strain. The steel strain is an important index in the experiment of reinforced concrete structures and it also plays an important role in the analysis of the stress performance of reinforced concrete beam-to-column joints. Figure 14 and 15 show the strain-load curve of the longitudinal reinforcement at the beam end and the strain-load curve of the stirrup in the core area of the joint, respectively.

As shown in Figure 14, when specimens are in the elastic stage, the strain value of the longitudinal reinforcement of those is small. The development trends of those are roughly the same, and they are basically linear. In Figure 14(a), when the load increases to 40 kN (yield load), the strain value of the longitudinal bars of the specimen RCJ-19-0.12 is 2000 $\mu\varepsilon$, the longitudinal bars have yielded. The strain value of the longitudinal reinforcements of specimen RCJ-50-19-0.12 is 1600 $\mu\varepsilon$; the longitudinal reinforcements just reach the yielding state. The strain value of the longitudinal bars of the specimen RCJ-100-19-0.12 is 1100 $\mu\varepsilon$, and the longitudinal bars do not reach the yielding state. In Figure 14(b), when the load increases to 40 kN (yield load), the strain value of the longitudinal bars of the specimen RCJ-50-19-0.12 and the specimen RCJ-50-19-0.16 is about 1700 $\mu\varepsilon$, and the longitudinal bars have yielded. The strain value of the longitudinal reinforcements of RCJ-50-19-0.08 is about 1200 $\mu\varepsilon$, and the longitudinal reinforcements do not reach the yield state. In Figure 14(c), when the load increases to about 40 kN (yield load), the strain value of the longitudinal bars of the specimen RCJ-50-12-0.12 and the specimen RCJ-50-19-0.12 is about 1600 $\mu\varepsilon$, and the longitudinal bars have yielded. The strain value of the longitudinal reinforcements of the specimen RCJ-50-30-0.12 is about 1200 $\mu\varepsilon$, and the longitudinal reinforcements do not reach the yield state. Among them, the volume of waste fibers has the more obvious effect on reducing the strain of steel bars and delaying the yield of longitudinal bars. The waste fibers improve the shear resistance of concrete by improving the occlusal ability of aggregates on the section. The waste fibers and the steel bar bear the tensile force of the beam. When the specimen is damaged, the waste fibers are broken and pulled out (see Figure 10). The waste fibers can achieve the effect of reducing the stress and strain of the tension main reinforcement and delay the yield of steel reinforcements.

During the failure process of the specimens, no shear oblique cracks appeared in the core area of the joint. At this time, the stirrups of the joint can better constrain the concrete in the core area, effectively inhibiting the generation of oblique cracks in the core area of the joint, and reducing the shear deformation of the concrete.

As shown in Figure 15(a), when the load is in the 0–20 kN range, the strain of stirrups in the core area of specimens NCJ, CJ-19-0.12, and RCJ-100-19-0.12 remains almost unchanged. The strain rate of the stirrup in the core area of the specimen RCJ-50-19-0.12 accelerates. When the load reaches 30 kN, the strain of the stirrup in the core area of the specimen RCJ-50-19-0.12 is about 100 $\mu\varepsilon$, and the strain of the stirrup in the core area of the specimen NCJ, the specimen RCJ-19-0.12, and the specimen RCJ-100-19-0.12 is about 18 $\mu\varepsilon$. When the load reaches 50 kN, the strain of the stirrup in the core area of the specimen RCJ-50-19-0.12 is about 458 $\mu\varepsilon$.

As shown in Figure 15(b), when the load is in the 0–20 kN range, the strain change of the stirrups in the core area of the specimens RCJ-50-19-0.08 and RCJ-50-19-0.16 is very small. And the stirrups in the core area of the specimen RCJ-50 -19-0.12 are roughly linear with the increase of the load. When the load reaches 40 kN, the strain value of the

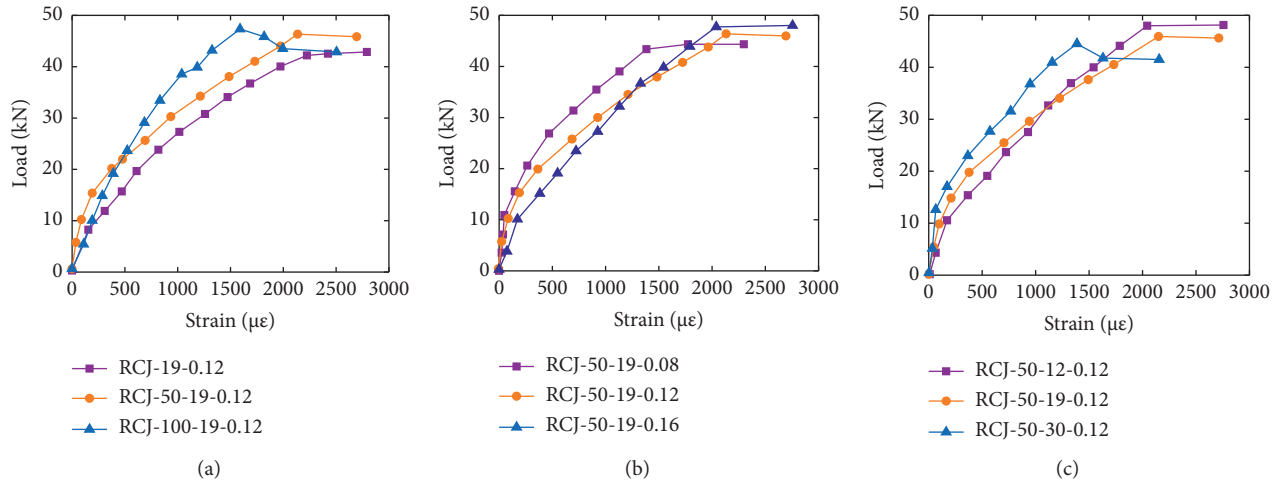

Figure 14: Comparison of influencing factors of strain-load curve of longitudinal reinforcement at beam end. (a) Replacement rate of RCA. (b) Volume of waste fibers. (c) Length of waste fibers.

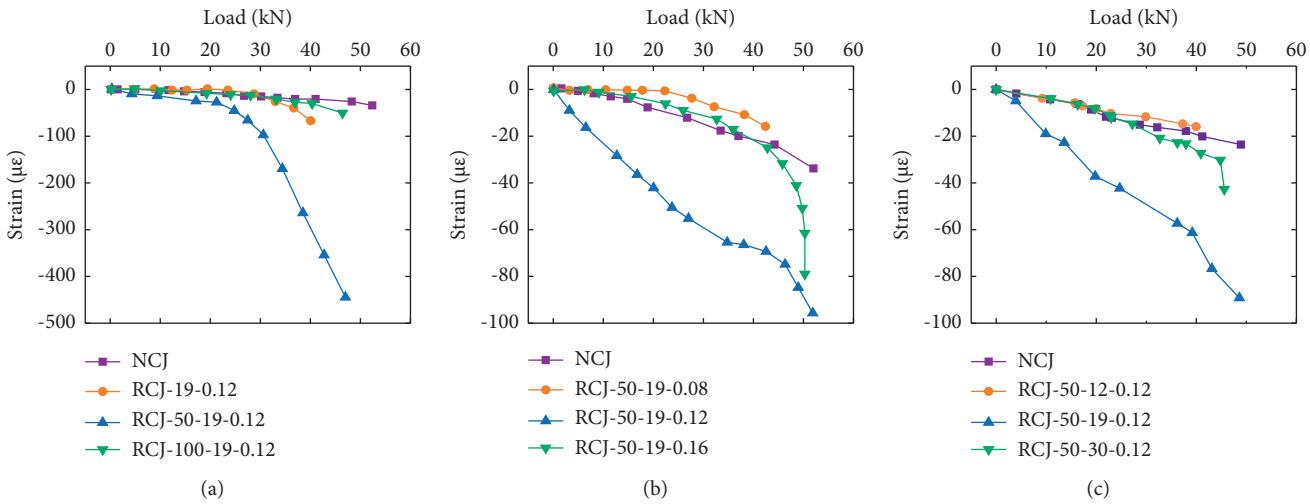

Figure 15: Comparison of influencing factors of stirrup strain-load curve. (a) Replacement rate of RCA. (b) Volume of waste fibers. (c) Length of waste fibers.

stirrups is about 20 $\mu\varepsilon$. When the load increases from 40 kN to 50 kN, the strain increase of the stirrups in the core area of the specimens RCJ-50-19-0.08 and RCJ-50-19-0.16 suddenly increases to 90 $\mu\varepsilon$.

As shown in Figure 15(c), when the load is in the 0–20 kN range, the strain change of the stirrups in the core area of the specimens RCJ-50-12-0.12 and RCJ-50-30-0.12 is smaller with the increase of the load. It coincides with the curve of the specimen NCJ. The strain of the stirrup in the core area of the specimen RCJ-50-19-0.12 is roughly linear with the increase of the load. When the load reaches 40 kN, the strain value of the stirrup is about 60 $\mu\varepsilon$. The maximum strain of the reinforcement is 80 $\mu\varepsilon$. When the load reaches 40 kN, the strain value of the stirrups is about 20 $\mu\varepsilon$. The maximum strain of the stirrups is only 80 $\mu\varepsilon$.

In summary, the maximum strain value of the stirrups in the core area of all the above specimens is less than the yield strain of the stirrups. It indicates that the stirrups are always in the elastic stage during the entire loading process and can constrain the concrete in the core area. Through the controlled variable method, it can be seen that the suitable value of the replacement rate of RCA is about 50%, that of the waste fiber volume fraction is about 0.12, and that of the waste fiber length is about 19 mm, regardless of whether the variables are greater or less than the suitable value, which has little effect on the strain of the stirrup in the core area of the joint.

4.5. Calculation of Ultimate Bearing Capacity of Beam-to-Column Joint. The calculation method of the ultimate bearing capacity of the normal section of recycled concrete members is based on GB50010-2010 (Chinese standard). The design strength of recycled concrete in the corresponding

calculation formula should be multiplied by the reduction factor k_1, when the replacement rate of RCA is 50%, $k_1 = 0.85$, and when the replacement rate of RCA is 100%, $k_1 = 0.75$.

According to the relevant regulations in CECS 38: 2004 (Chinese standard), the calculation principle of the bearing capacity of the positive section of fiber-reinforced concrete members is as follows: the basic calculation model can adopt the relevant provisions of the concrete structure design joint, but the residual tensile stress of the fiber concrete in the tension zone of the beam end should be considered in the ultimate state.

The residual tensile stress of the fiber concrete in the tensile zone at the cross section can be simplified into an equivalent rectangular stress distribution diagram. The calculation formula for the tensile stress f_{ftu} of the equivalent rectangular stress graph and the height of tensile zone x_t is as follows:

$$\begin{aligned} x_t &= h - \frac{x}{\beta_1}, \\ f_{ftu} &= f_t \beta_{tu} \lambda_f. \end{aligned} \tag{2}$$

where λ_f denotes the characteristic content parameter of the waste fibers; x is the compression zone height of the concrete cross-section; β_1 is the ratio of the compression zone height of the equivalent rectangular stress pattern to the distance from the neutral axis to the compression edge; and β_{tu} is the influence coefficient of the tensile effect of the fibers in the compression zone of waste fiber concretes in the tension zone.

The compressive stress-strain model and related parameters of fiber concrete can be adopted approximately in accordance with the regulations of ordinary concrete, and the stress graph of the compression zone of the normal section can also be adopted in accordance with the relevant regulations in GB50010-2010 (Chinese standard). The stress-strain relationship curve of recycled concrete adopts an idealized stress-strain curve. The first section (ascending section), when $\varepsilon_c \le \varepsilon_0$, is as follows:

$$\begin{aligned} \sigma_c &= f_c \left[1 - \left(1 - \frac{\varepsilon_c}{\varepsilon_o} \right)^2 \right]^n, \\ n &= 2 - \frac{1}{60} (f_{cu} - 50). \end{aligned} \tag{3}$$

The second section (horizontal section), when $\varepsilon_0 < \varepsilon_c \le \varepsilon_{cu}$, is as follows:

$$\begin{aligned} \sigma_c &= f_c, \\ \varepsilon_o &= 0.002 + 0.5 (f_{cu} - 50) \times 10^{-5}, \\ \varepsilon_{cu} &= 0.0033 + (f_{cu} - 50) \times 10^{-5}. \end{aligned} \tag{4}$$

where σ_c denotes the compressive stress of concrete when the strain of recycled concrete is ε_c and ε_o denotes the compressive strain of recycled concrete when the compressive stress of recycled concrete reaches f_c. When the calculated value ε_o is less than 0.002, it should be taken as 0.002. Term ε_{cu} denotes the ultimate compressive strain of recycled concrete when the normal section is under non-uniform compression. When the calculated ε_{cu} is greater than 0.0033, it should be taken as 0.0033. Term f_{cu} denotes the standard value of the cubic compressive strength of recycled concrete and n is the coefficient: when the calculated n is greater than 2.0, it should be 2.0. The values of n, ε_0, and ε_{cu} are listed in Table 5.

The stress-strain relationship equation of the steel bar is

$$\sigma_s = E_s \cdot \varepsilon_s \le f_y. \tag{5}$$

The ultimate tensile strain of the tensile steel bar is taken as 0.01. When $\varepsilon_0 \le \varepsilon_s \le \varepsilon_y$, $\sigma_s = E_s \cdot \varepsilon_s$; $\varepsilon_s > \varepsilon_y$, $\sigma_s = f_y$.

According to GB50010-2010 (Chinese standard), the calculation of the ultimate flexural bearing capacity of concrete symmetrically reinforced beams and the average stress of the compressive longitudinal reinforcement cannot reach the yield strength. Term P denotes the vertical force applied to the outer end of the beam, and L denotes the horizontal distance from the point of application of P to the beam root (the edge of the joint). The force diagram is shown in Figure 16.

According to the static balance conditions, the following two static balance equations are established:

$$\begin{aligned} \sum X &= 0 \alpha_1 f_{tc} b x + \sigma_s' A_s' = f_y A_s + f_{ftu} b x_t, \\ \sum M &= 0 Pl = \alpha_1 f_c b x \left(h_0 - \frac{x}{2} \right) + \sigma_s' A_s' (h_0 - \alpha')_s. \end{aligned} \tag{6}$$

where $\alpha_1 = 0.95$ represents the ratio of stress value of the rectangular stress diagram in the compression area to design the value of axial compressive strength, x and x_t represent the height of compression and tension zone of beam (mm), f_{tc} represents the design value of axial compressive strength of recycled concrete(MPa), f_y and σ_s' represent tensile and compressive design strength of longitudinal reinforcement (MPa), α_s and α_s' represent the distance from resultant force point of tension and compression longitudinal reinforcement to section edge (mm), A_s and A_s' represent the sectional area of tension and compression longitudinal reinforcement (mm^2), and P denotes the ultimate bearing capacity of beam end (kN).

After incorporating the corresponding calculation results into (6), the ultimate bearing capacity P of the beam end can be determined. The calculation results are summarized in Table 6, where P is the calculated value of the ultimate bearing capacity of the beam end and P' is the test value of the ultimate bearing capacity of the beam end.

As shown in Table 6, the ratio of the calculated value to the test value is in the 0.96–1.10 range, and it is in good agreement with the test value. The assumption that the influence coefficient $\beta_{tu} = 1.15$ of the waste fibers for the tensile effect of the fiber concrete in the tension zone is confirmed.

Table 5: The values of n, ε_0, and ε_{cu}.

Series	≤C50	C50	C60	C65	C70	C75	C80
n	2	1.917	1.833	1.75	1.667	1.583	1.5
ε_0	0.002	0.00202	0.00205	0.00207	0.0021	0.00212	0.00215
ε_0	0.0033	0.0032	0.0032	0.0031	0.0031	0.003	0.003

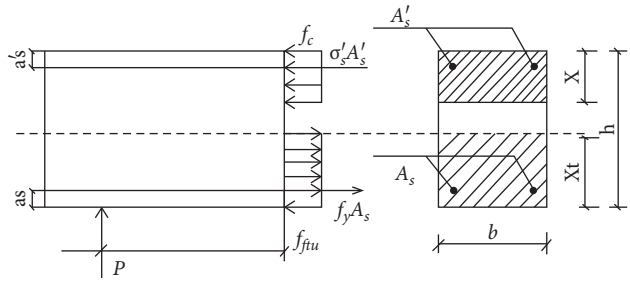

Figure 16: Schematic diagram of predigest calculation.

Table 6: Calculation value P and test value P' of ultimate bearing capacity of column-beam joints.

Specimen ID	Waste fibers		β_{tu}	Replacement rate of recycled aggregates (%)	k_1	P/kN	P'/ kN	P/P'
	Length (mm)	Volume incorporation (%)						
NCJ	0	0	0	0	1	54.98	52.70	1.04
RCJ-50-19-0.12	19	0.12	1.15	50	0.85	49.18	50.92	0.96
RCJ-50-12-0.12	12	0.12	1.15	50	0.85	48.32	47.65	1.01
RCJ-50-30-0.12	30	0.12	1.15	50	0.85	51.37	43.35	1.08
RCJ-19-0.12	19	0.12	1.15	0	1	56.01	53.82	1.04
RCJ-100-19-0.12	19	0.12	1.15	100	0.75	46.34	46.30	1.01
RCJ-50-19-0.08	19	0.08	1.15	50	0.85	47.06	43.10	1.09
RCJ-50-19-0.16	19	1.16	1.15	50	0.85	52.37	48.94	1.07

5. Conclusions

The following conclusions can be drawn from experimental and analytical investigations:

(1) The incorporation of RCA is unfavorable to the ultimate load-bearing capacity of waste fiber recycled concrete beam-column joints. However, when the amount of RCA is 50%, adding a specific amount of fibers can effectively improve the tensile strength of the concrete. The ultimate bearing capacity of RCJ-50-19-0.12 was 9.6% and 11.22% higher than those of RCJ-19-0.12 and RCJ-100-19-0.12, respectively, which are close to that of NCJ.

(2) The waste fibers are used as the "secondary reinforcement" of the concrete to redistribute the stress of the concrete within the saturation of the fibers. They are broken and pulled out during the bending process of the beam end, and this consumes a part of the energy of the concrete bending in the joint area, thereby increasing the ultimate bearing capacity of the beam end. The test results demonstrated that the saturation value was 0.12%. When the saturation value exceeds 0.12%, the ultimate bearing capacity decreases or the increasing trend is weakened.

(3) The waste fibers had a small diameter and moderate fiber length. After mixing, they were evenly dispersed and distributed in a three-dimensional chaotic manner in the concrete. The fibers were in a bent state, which increased the bonding strength between the fibers and concrete, delayed the generation of cracks, and controlled the development of cracks, consequently enhancing the load-bearing performance of the beam ends in the joint area. The test showed that when the waste fiber length was 19 mm, the ultimate load-bearing performance of the beam end was the best.

(4) According to the comparative analysis between the calculation and test results of the ultimate bearing capacity of the beam end of the waste fiber recycled concrete beam-column joints, the ratio between the calculated and test values is in the 0.96–1.10 range, and the calculated solution coincides well with the data during the test. The assumption that the fiber influence coefficient $\beta_{tu} = 1.15$ on the tensile effect of the fiber concrete in the tension zone is confirmed.

Notation

RCA: Recycled coarse aggregates
NCA: Natural coarse aggregates
δ_1, δ_2, δ_3, δ_4: The variations in the length
k_1: The reduction factor
f_{ftu}: The tensile stress of the equivalent rectangular stress graph
x_t: The height of tensile zone
x: The height of compression zone
λ_f: The characteristic content parameter of the waste fibers
β_1: The ratio of the compression zone height of the equivalent rectangular stress graph
β_{tu}: The influence coefficient of the tensile effect of the fibers in the compression zone
σ_c: The compressive stress of recycled concrete
ε_c: The compressive strain of recycled concrete
ε_{cu}: The ultimate compressive strain of recycled concrete
f_{cu}: The cubic compressive strength of recycled concrete
f_{tc}: The axial compressive strength of recycled concrete
f_y: The tensile strength of longitudinal reinforcement
σ_s': The compressive strength of longitudinal reinforcement
A_s: The sectional area of tension longitudinal reinforcement
A_s': The sectional area of compression longitudinal reinforcement
P: The ultimate bearing capacity
P': The test value of the ultimate bearing capacity.

Data Availability

The data used to support the findings of the study are included within the manuscript.

Conflicts of Interest

No potential conflicts of interest are reported by the authors.

Acknowledgments

This work was supported by the National Natural Science Foundation of China (nos. 52108235 and 51678374), Fundamental Research Funds for the Central Universities (no. 300102341511), and Liaoning Provincial Department of Education Fund (nos. lnqn202003 and LT2019011). The financial support is gratefully acknowledged.

References

[1] L. Li, Z. F. Li, X. D. Li, S. X. Zhang, and X. W. Luo, "A new framework of industrialized construction method in China: towards on-site industrialization," *Journal of Cleaner Production*, vol. 244, Article ID 118469, 2019.

[2] X. Zhang and M. Skitmore, "Industrialized Housing in China: a Coin with two sides," *International Journal of Strategic Property Management*, vol. 16, no. 2, pp. 143–157, 2012.

[3] J. Z. Xiao, J. L. Wang, Z. P. Sun, and J. B. Li, "Research on application of recycled coarse aggregate in cement concrete pavement," *Highway Traffic Technology*, vol. 22, no. 9, pp. 52–55, 2005.

[4] D. Meng, X. M. Wu, H. Z. Quan, and C. J. Zhu, "A strength-based mix design method for recycled aggregate concrete and consequent durability performance," *Construction and Building Materials*, vol. 281, Article ID 122616, 2021.

[5] M. Etxeberria, E. Vázquez, A. Marí, and M. Barra, "Influence of amount of recycled coarse aggregates and production process on properties of recycled aggregate concrete," *Cement and Concrete Research*, vol. 37, no. 5, pp. 735–742, 2007.

[6] C. S. Poon, Z. H. Shui, L. Lam, H. Fok, and S. C. Kou, "Influence of moisture states of natural and recycled aggregates on the slump and compressive strength of concrete," *Cement and Concrete Research*, vol. 34, no. 1, pp. 31–36, 2004.

[7] J. A. Carneiro, P. R. L. Lima, M. B. Leite, and R. D. Toledo Filho, "Compressive stress-strain behavior of steel fiber reinforced-recycled aggregate concrete," *Cement and Concrete Composites*, vol. 46, no. 4, pp. 65–72, 2014.

[8] S. Yin, R. Tuladhar, R. A. Shanks et al., "Fiber preparation and mechanical properties of recycled polypropylene for reinforcing concrete," *Journal of Applied Polymer Science*, vol. 41866, pp. 1–10, 2015.

[9] J. H. Zhou, T. B. Kang, and F. C. Wang, "Pore structure and strength of waste fiber recycled concrete," *Journal of Engineered Fibers and Fabrics*, vol. 14, pp. 1–10, 2019.

[10] M. J. Shannag, N. Abu-Dyya, and G. Abu-Farsakh, "Lateral load response of high performance fiber reinforced concrete beam-column joints," *Construction and Building Materials*, vol. 19, no. 7, pp. 500–508, 2005.

[11] P. Saranya, P. Nagarajan, and A. P. Shashikala, "Behaviour of GGBS-dolomite geopolymer concrete beam-column joints under monotonic loading," *Structures*, vol. 25, pp. 47–55, 2020.

[12] M. Nehdi, M. S. Alam, and M. A. Youssef, "Development of corrosion-free concrete beam-column joint with adequate seismic energy dissipation," *Engineering Structures*, vol. 32, no. 9, pp. 2518–2528, 2010.

[13] M. A. Najafgholipour and A. R. Arabi, "A nonlinear model to apply beam-column joint shear failure in analysis of RC moment resisting frames," *Structures*, vol. 22, pp. 13–27, 2019.

[14] C. Marthong, A. S. Sangma, S. A. Choudhury, R. N. Pyrbot, S. L. Tron, and L. G. S. S. Bharti, "Structural behavior of recycled aggregate concrete beam-column connection in presence of micro concrete at joint region," *Structures*, vol. 11, pp. 243–251, 2017.

[15] C. Viviana, L. Gonzalez, and G. Moriconi, "The influence of recycled concrete aggregates on the behavior of beam–column joints under cyclic loading," *Engineering Structures*, vol. 60, pp. 148–154, 2014.

[16] B. Hu and T. Kundu, "Seismic performance of interior and Exterior beam-column joints in recycled aggregate concrete frames," *Journal of Structural Engineering*, vol. 145, no. 3, Article ID 04018262, 16 pages, 2019.

[17] V. Corinaldwsi, V. Letelier, and G. Moricobi, "Behavior of beam-column joints made of recycled-aggregate concrete under cyclic loading," *Construction and Building Materials*, vol. 25, no. 4, pp. 1877–1882, 2011.

[18] Y. K. Peng, H. Wu, and N. S Liang, "Mechanical performance of middle joints of recycled concrete frame under low-cycle

cyclic loading," *World Earthquake Engineering*, vol. 30, no. 3, pp. 86–92, 2014.

[19] C. Liu, G. L. Bai, and S. W. Jia, "Experimental study on seismic performance of recycled concrete frame joints with different axial compression ratios," *China Civil Engineering Journal*, vol. 46, no. 6, pp. 21–28, 2013.

[20] J. Su, J. P. Liu, W. Li, and M. Chen, "Experimental research of shear behavior of frame joints by fiber reinforced concrete under reversed cyclic loading," *Journal of Earthquake Engineering and Engineering Vibration*, vol. 36, no. 2, pp. 36–41, 2016.

[21] Y. F. Du and S. L. Wang, "Experimental research on seismic bearing performance of fiber composite reinforced recycled concrete frame joints," *Journal of Building Structures*, vol. 37, no. 4, pp. 40–46, 2016.

[22] L. Candido and F. Micelli, "Seismic behavior of regular reinforced concrete plane frames with fiber reinforced concrete in joints," *Bulletin of Earthquake Engineering*, vol. 16, no. 9, pp. 4107–4132, 2018.

[23] T. Y. Wang, Y. Zhou, and J. W. Zhang, "Seismic behavior analysis of damaged steel fiber-reinforced high-strength concrete frame joints strengthened by FRP," *Advances in Civil Engineering*, vol. 2020, Article ID 8836516, 13 pages, 2020.

[24] N. F. Hany, E. G. Hantouche, and M. H. Harajili, "Axial stress-strain model of CFRP-confined concrete under monotonic and cyclic loading," *Journal of Composites for Construction*, vol. 19, no. 6, Article ID 4015004, 2015.

[25] S. K. Ghomi and E. El-Salakawy, "Effect of joint shear stress on seismic behaviour of interior GFRP-RC beam-column joints," *Engineering Structures*, vol. 191, pp. 583–597, 2019.

[26] E. I. Saqan, H. A. Rasheed, and T. Alkhrdaji, "Seismic behavior of carbon fiber-reinforced polymer-strengthened reinforced concrete members with various anchors," *ACI Structural Journal*, vol. 117, no. 4, pp. 3–14, 2020.

[27] C. G. Karayannis and E. Golias, "Full scale tests of RC joints with minor to moderate seismic damage repaired using C-FRP sheets," *Earthquakes and Structures*, vol. 15, no. 6, pp. 617–627, 2018.

[28] C. G. Karayannis and E. Golias, "Strengthening of deficient RC joints with diagonally placed external C-FRP ropes," *Earthquakes and Structures*, vol. 20, no. 1, pp. 123–132, 2021.